Volume 23
Number 11
7 June 2023
Pages 2489–2684

Lab on a Chip

Devices and applications at the micro- and nanoscale

rsc.li/loc

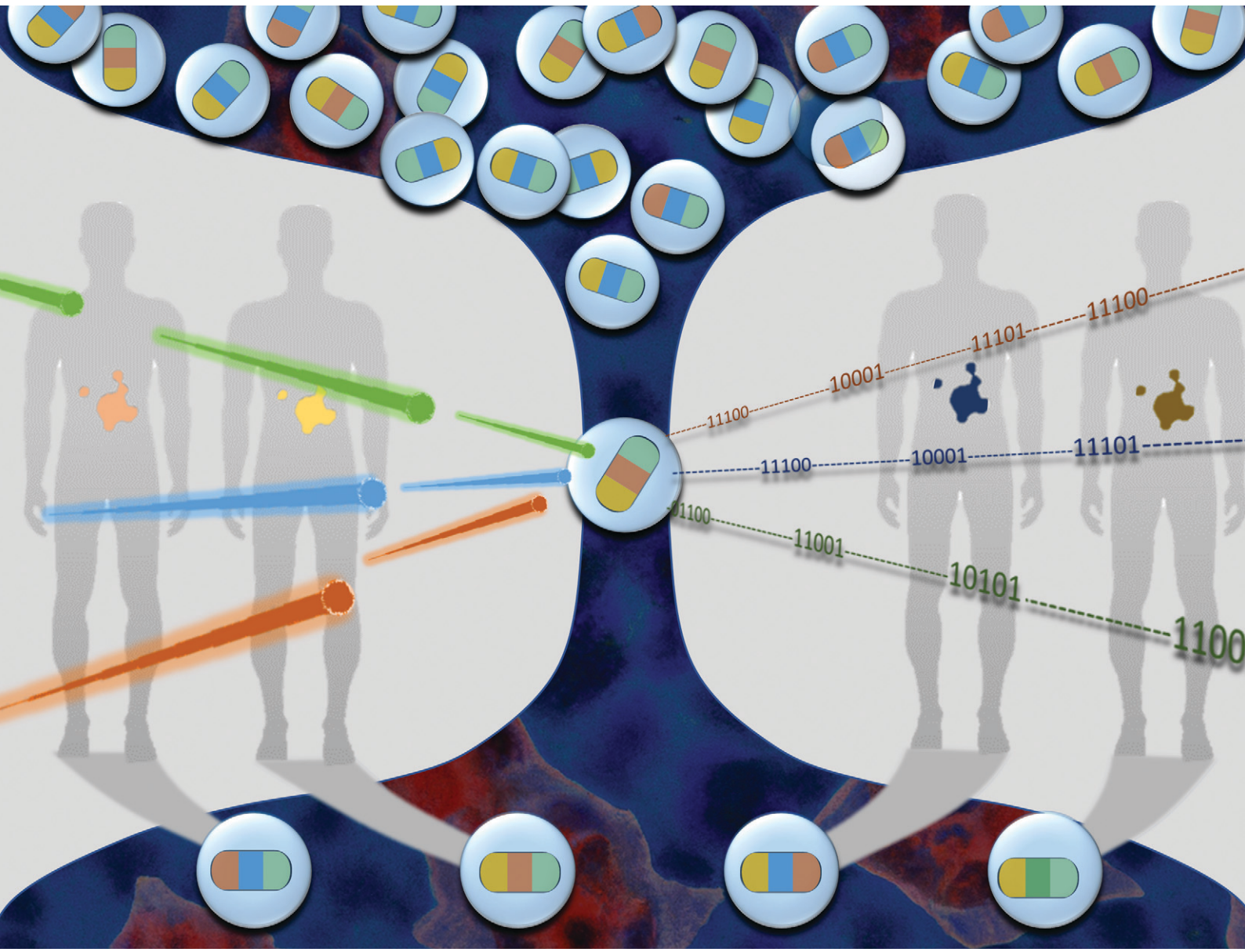

ISSN 1473-0197

ROYAL SOCIETY OF CHEMISTRY

COMMUNICATION

Jatin Panwar and Christoph A. Merten
Fluorescence crosstalk reduction by *modulated excitation-synchronous acquisition* for multispectral analysis in high-throughput droplet microfluidics

Lab on a Chip

COMMUNICATION

View Article Online
View Journal | View Issue

Cite this: *Lab Chip*, 2023, **23**, 2514

Received 2nd November 2022,
Accepted 27th April 2023

DOI: 10.1039/d2lc01016j

rsc.li/loc

Fluorescence crosstalk reduction by *modulated excitation-synchronous acquisition* for multispectral analysis in high-throughput droplet microfluidics†

Jatin Panwar [ab] and Christoph A. Merten *[a]

Crosstalk between fluorescent biomarkers significantly limits the resolution of multispectral fluorescence analysis in real-time droplet-microfluidics applications. The crosstalk is a result of overlapping emission and excitation spectra of different fluorophores in multiplexed analyses. To mitigate this crosstalk, we present a method that modulates multiple laser beams to selectively and sequentially excite the fluorophores by a single beam of a particular wavelength using acousto-optic modulators at a frequency of 0.1 MHz. An FPGA based data acquisition algorithm synchronized with the modulation signal then acquires the emission signals only from the fluorescence channel that corresponds to the excitation wavelength provided in that particular time window. We applied our method for fluorescence-based droplet analysis in microfluidics and demonstrate that the method is able to reduce crosstalk contribution between channels by >97% and can resolve fluorescence populations that are indistinguishable with conventional droplet analysis methods.

Fluorescence analysis has been the backbone of biochemical quantification, allowing the specific labelling and monitoring of analytes of interest, optionally in a highly multiplexed way. Droplet microfluidics benefits from these fluorescence analysis principles for compartmentalized quantification of cellular/molecular interactions, enzymatic activities and the level of secreted metabolites and antibodies.[1–3] Even though the wide range of available fluorescent biomarkers with varying excitation and emission spectra presents the possibility of high precision multispectral analysis, the caveat lies in the overlap between their spectra, resulting in crosstalk that significantly limits resolution. There are numerous solutions suggested in literature to overcome this issue for various fluorescence analysis techniques like Fluorescence Correlation Spectroscopy (FCS), Fluorescence Resonance Energy Transfer (FRET), widefield fluorescence imaging, Fluorescence Activated Cell Sorting (FACS) and Imaging Mass Cytometry (IMC).[4–7] A popular solution is to use numerical correction factors to compensate for the extra signal contributed by the crosstalk.[7,8] These correction factors are usually estimated before the analysis as calibration exercises for specific fluorescence targets and excitation sources that can later be applied in real-time experiments. A prerequisite of such precalculated correction factors is that the fluorescence targets stay at the same position in relation to the excitation source (*i.e.* the focal point of laser) during the experiment as they were during the calibrations. However, due to the peculiar nature of droplets that do not allow their contents to have fixed positions within the droplet volume, such precalculated correction factors are not suitable to compensate crosstalk in droplet microfluidics.[9] Some methods also conduct post experiment data cleaning to compensate for crosstalk like in case of IMC,[7] but such methods are not feasible for applications like droplet sorting, requiring real-time data analysis for decision making.[10–12] As a result, currently all fluorescence based droplet analysis methods suffer from limited signal resolution due to crosstalk.[10,13] To overcome these limitations, it is advantageous to apply means that evade the factors that cause crosstalk in the first place, rather than compensating for it once it has originated. These factors: 1) overlap of emission spectra of two fluorophores, 2) overlap of excitation spectra of a fluorophore with other channel's excitation wavelength and 3) overlap of excitation spectra of one fluorophore with the emission spectra of another fluorophore (*i.e.* due to Förster resonance energy transfer (*FRET*) between two fluorophores).[14]

We present a method called "*Modulated Excitation-Synchronous Acquisition*" or MESA that allows sequential and selective modulation of excitation signals *i.e.* lasers, that are also synchronized with the data acquisition from emission

[a] *Institute of Bioengineering, School of Engineering, École Polytechnique Fédérale de Lausanne (EPFL), Lausanne, Switzerland. E-mail: christoph.merten@epfl.ch*
[b] *European Molecular Biology Laboratory (EMBL), Heidelberg, Germany*
† Electronic supplementary information (ESI) available. See DOI: https://doi.org/10.1039/d2lc01016j

channels. The sequential modulation of laser beams ensures that only the fluorophore whose excitation spectra corresponds to the laser beam that is "on" in that moment is excited, so that the acquired emission signals will not have the component from the other fluorophores. The modulated excitation eliminates the crosstalk due to emission spectra overlap as also shown in literature.[5,15] However, the crosstalk still persists at this point as a single laser can also partially excite multiple fluorophores due to FRET from the excited "correct" fluorophore or due to the overlap of excitation spectra of "incorrect" fluorophores with the laser (typically, the excitation spectrum of all fluorophores is extended towards the low wavelengths). This results in higher than expected emission from the fluorophores that do not correspond to the "on" laser. Additionally, the emission from the fluorophore corresponding to the "on" laser may still leak into other channels further increasing the crosstalk. To avoid such crosstalk components, it is essential to modulate PMTs in sync with the lasers, such that only a single laser and its corresponding PMT is "on" at any given time. This creates discontinuity (*i.e.* time intervals with no signal which attenuate the mean signal amplitude) in the signals acquired from the PMTs which has to be processed computationally by MESA for perfect synchronization without signal loss. This way, MESA integrates sequential modulation with synchronized emission data acquisition to eliminate all three critical components of crosstalk.

We applied this method to conduct fluorescence analysis in high-throughput droplet microfluidics to demonstrate the crosstalk reduction in the signals obtained with MESA mode as compared to the same signals obtained in unmodulated or continuous wave (CW) mode. CW mode is currently used in all droplet analysis methods and thus, provides an excellent benchmark for comparison.[9,10,12,16–18] We further demonstrate that due to the improved crosstalk reduction, MESA can separate fluorescence populations that otherwise remain indistinguishable. We, thus, envisage that our method can become an integral part of highly multiplexed applications in life science and biomedicine.

We used three acousto-optic modulators (AOM) for sequential modulation of three continuous-wave laser beams of wavelengths 405 nm, 473 nm and 561 nm (Fig. 1a). We used commercially available laser assembly that comes with inbuilt AOMs, which can be controlled computationally *via* TTL pulses (Jilin Laser Tech. Ltd., China). This also makes implementation of MESA easier and cost effective in comparison to standard multi-wavelength droplet analysis platforms that require laser alignment and additional optical components.[12] For signal modulation, data acquisition and

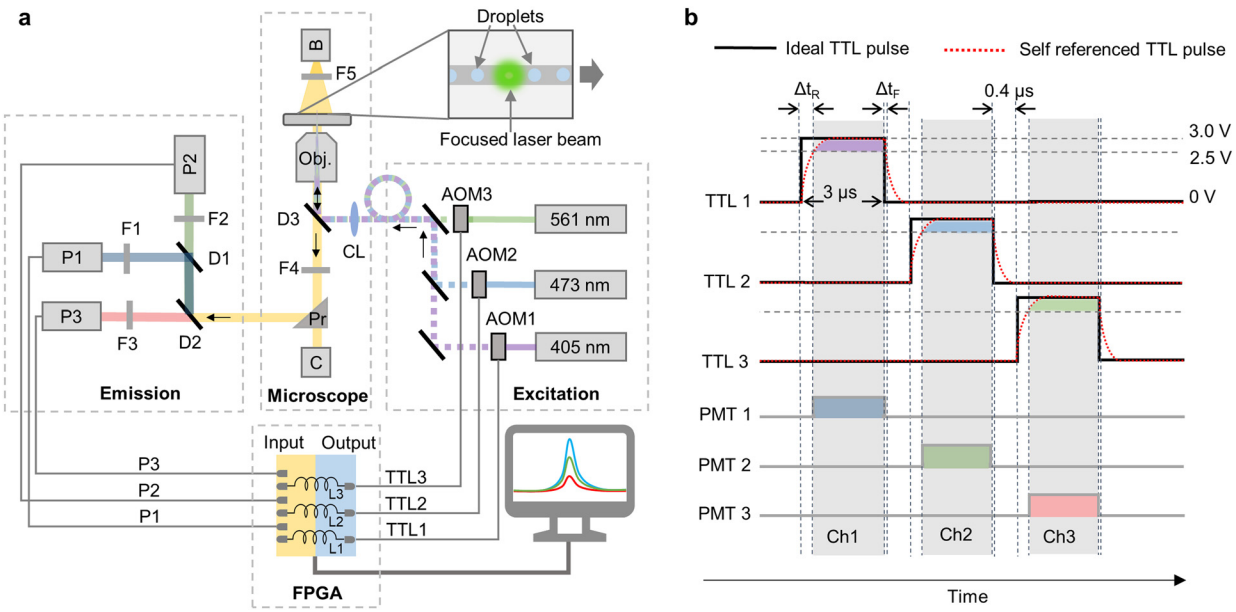

Fig. 1 Modulated excitation-synchronous acquisition (MESA) setup. a) Optical setup with three laser beams (561 nm, 473 nm and 405 nm wavelengths) that are combined and sent to the microscope through an optical fiber cable after acousto-optic modulation (AOM1–3). A convex lens (CL) of 100 mm focal length is used to converge the laser beam on the microscope's objective lens *via* a dichroic mirror (D3: 403/497/574 nm triple beam splitter). The modulated beams excite the droplets and the subsequent emission passes through a laser cleanup filter (F4: 405/473/561 nm triple band notch filter) before separating into three channels using dichroic mirrors (D1: 484 nm and D2: 552 nm beam splitters) and collected by three photomultiplier tubes (P1–P3). The optical filters (F1: 445/45 nm, F2: 525/45 nm and F3: 605/40 nm bandpass) in front of each PMT further clean the emission signal and define the channel bandwidth. The FPGA connections show TTL pulse outputs and PMT signal inputs along with the connection for self-reference signal (L1–3). The camera (C) images the sample which is illuminated by the brightfield lamp (B). To prevent this illumination from interfering with the emission signals, an optical filter (F5: 630 nm high-pass) is placed after the brightfield lamp. b) Composition of TTL pulses with a pulse width of 300 ns sent to the AOMs for switching the laser to the desired "on" state at TTL $>$ 2.5 V. The time delay between ideal TTL pulse and self-reference signal due to rise time is Δt_R while Δt_F is the delay due to fall time.

real-time analysis, a custom-made FPGA algorithm was designed using LabVIEW FPGA module running on a NI PXIe 7856R FPGA card with a sampling rate of 40 MHz. The algorithm sequentially generates separate TTL (transistor–transistor logic) pulses with PWM (pulse-width modulation) for each AOM at a frequency of ~100 kHz with low and high amplitudes of 0 V and 3 V respectively (Fig. 1b). The TTL pulses had an "on" time of 3 μs and were separated by 400 ns to avoid any signal leakage due to the fluorescence lifetime of fluorophores[19] resulting into a complete pulse cycle of 10.2 μs during which, 120 datapoints for each laser excitation can be acquired by the FPGA that is running at a sampling rate of 40 MHz. The modulated laser beams then excite the fluorophores in the droplets *via* a fiber-optic cable. The subsequent emission signals are separated in three channels (Ch 1: blue, 425 nm to 465 nm; Ch 2: green, 505 nm to 545 nm and Ch 3: red, 580 nm to 620 nm) and are captured by three photomultiplier tubes (PMT). The details of optical components and their placement is shown in the ray diagram in Fig. 1a. The signals from PMTs are then acquired in synchronization with the modulation signal, such that only the PMT for which the corresponding excitation beam is "*on*" in that moment is read (Fig. 1b). The synchronization, however cannot be efficient unless the time delay due to the rise/fall time and slew rate of TTL pulse generation and due to the inductance of the cable connecting the FPGA to AOM is considered. To compensate for this delay, the modulation signals that are sent to each AOM are parallelly connected to analog inputs of FPGA and acquired as "*self-reference*". The PMT synchronization is based on the rise time of this "*self-reference signal*" (Fig. 1b). Since the fall-time follows the exponential decay function and the TTL high cutoff (2.5 V) of the AOM trigger is close to TTL high (3 V), the delay between the TTL pulse and the self-reference signal at TTL fall (Δt_F) is significantly small as compared to TTL rise (Δt_R). Therefore, the algorithm considers the falling TTL pulse's timepoint to synchronize emission signal acquisition in that channel (Fig. 1b).

We first compared the droplet fluorescence signals acquired by MESA with the similar signals acquired using continuous wave (CW) excitation. For an efficient comparison, our custom-made LabVIEW code is programed to work in both MESA mode and CW mode. In CW mode, the TTL pulses for all the AOMs are set at a constant 'high' at 3 V resulting in continuous excitation from lasers and continuous data acquisition from PMTs. The droplets are generated using a flow focusing droplet generator that has three aqueous phase inlets (Fig. 2a). Inlet 1 contained 1 μM cascade blue (CB) that is excited by 405 nm laser and its emission is captured in Ch 1; inlet 2 had 1 μM fluorescein (FL) that is excited by 488 nm laser and its emission is captured in Ch 2 and inlet 3 contained 1× PBS (Phosphate-buffered saline), which is the only nonfluorescent aqueous solution and is used to adjust the concentration of the other fluorophores (Fig. 2b). The fluorophores are selected such that the data acquired in Ch1 will have least crosstalk due to FRET induced loss of some of CB's emission to excite FL (Fig. 2b). On the other hand, Ch2 is expected to have the emission signal from FL after its excitation from L2 along with some crosstalk. The crosstalk in Ch2 is comprised of multiple components due to: i) overlap of CB's emission spectra with Ch2, ii) overlap of FL's excitation spectra with L1 and iii) overlap of CB's emission spectra with FL's excitation spectra resulting in FRET (Fig. 2b). Similarly, due to lack of any fluorophore that can be excited by 561 nm, any signal acquired in Ch3 will correspond to the crosstalk from Ch1 and/or Ch2 (Fig. 2b). The droplets are generated with HFE 7500 oil as continuous phase with a flowrate of 800 μL h^{-1} and the overall aqueous phase flow rate of 350 μL h^{-1}, resulting in generation of ~500 pL droplets at ~200 Hz with

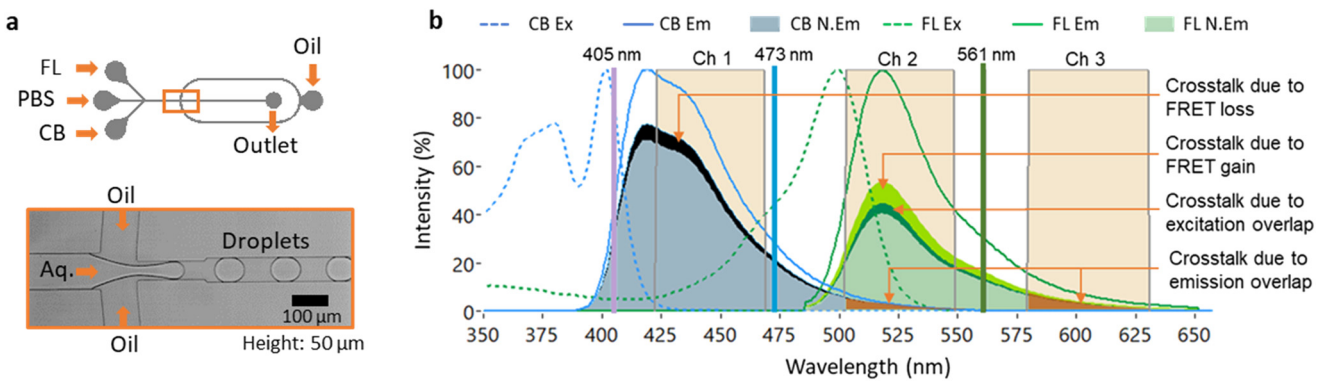

Fig. 2 Experimental setup. a) Microfluidic device used to generate droplets containing a mixture of fluorescein (1 μM), PBS (1×) and cascade blue (1 μM). b) Excitation (Ex) and emission (Em) spectra for the fluorophores cascade blue (CB) and fluorescein (FL). The normalized emission (N.Em) is the maximum emission (Em) multiplied by the extent of excitation (*i.e.* the intersection of laser with the excitation spectrum) and the quantum yield of the fluorophore (see Fig. S2† for further details). The laser wavelengths and its corresponding emission channel bandwidths are highlighted (Ch1: 423 nm to 468 nm, Ch2: 503 nm to 548 nm and Ch3: 580 nm to 620 nm). The crosstalk components due to spectral overlap and FRET are also highlighted. Ch2 is shown to have the multiple crosstalk components due to CB's emission spectrum overlapping with Ch2's bandwidth, 405 nm laser overlapping with FL's excitation spectra and FRET induced by the CB's emission spectra overlapping with FL's excitation spectra.

droplet width (the time spent by the droplet for passing the detection point) of 1.25 ± 0.2 ms (Video S1, Fig. S1†). This way, every excitation pulse of 3 μs excited every single droplet 122 times during its stay of 1.25 ms translating into ~14 k datapoints for each droplet for each channel which are more than sufficient for droplet fluorescence analysis even in conditions with high system noises. If we assume an ideal noise-free signal, even a single excitation cycle of 10.2 μs (*i.e.* 3 × [3 + 0.4] μs) is sufficient to acquire fluorescence signals in all three channels from a single droplet translating into a maximal theoretically possible throughput of ~49 kHz (where the droplets have a width of 10.2 μs with a gap of one droplet in between). This calculation indicates that our modulation frequency is orders of magnitude higher than what is required to analyze droplets moving at frequencies typically used in fluorescence analysis methods.[12] Such a high modulation frequency is a result of acousto-optic modulation and high-speed processing by FPGA, which cannot be achieved by conventional methods using filter wheels (minimum switching time of 25 ms)[20] and mechanical shutters (minimum switching time of 1 ms).[21]

To generate droplets with desired concentrations of fluorophores CB and FL, a custom-made LabVIEW code was used that stepwise changed the flow rates of syringe pumps and adjusted the ratios of the three different aqueous solutions (CB, FL and PBS). Once the desired ratio/concentration is reached, the code acquires data (*i.e.* amplitude of droplet fluorescence signal peaks) in both MESA mode and CW mode alternatively and then changes the flow rates again to reach the next concentration. This way, the program consistently generates droplets with discrete fluorophore concentrations while simultaneously acquiring the fluorescence signals in both modes from over 100 000 droplets in every population. A schematic of this automation algorithm is provided in Fig. S2.†

We generated droplet populations containing a stepwise increasing concentration of CB from 0.1–0.9 μM to analyze the crosstalk in Ch2 due to the spill over from Ch1 (Fig. 3a). Ideally, the slope of fluorescence signal amplitude in Ch2 as a function of CB concentration should be zero, and any non-zero slope is a consequence of crosstalk due to the overlap of CB's emission spectra with Ch2 bandwidth (Fig. 2b). This crosstalk can be quantified separately for both modes by calculating the crosstalk factor ($C_{i\to j}^{\text{mode}}$) *i.e.* the fraction of fluorescence signal acquired in channel i that is leaking into channel j averaged over all the 9 discrete concentrations:

$$C_{i\to j}^{\text{mode}} = \text{mean}\left[\frac{f_j^{\text{mode}}}{f_i^{\text{mode}}}\right] \quad (1)$$

here, f_i^{mode} is the mean amplitude of the droplet fluorescence signals at a particular concentration as obtained by the mode in consideration (MESA or CW) in channel i. The value of $C_{1\to 2}$ calculated using eqn (1) for MESA and CW signals is shown in Table 1. Similarly, $C_{2\to 3}$ was calculated by analyzing droplet fluorescence signals that had a stepwise increasing concentration of FL from 0.1 to 0.9 μM (Fig. 3b, Table 1). To calculate the crosstalk factors ($C_{1\to 3}$) for FRET induced crosstalk in Ch3 from Ch1, droplets with a constant FL concentration (0.5 μM) along with a stepwise increasing concentration of CB from 0.1–0.9 μM were analyzed (Fig. 3c, Table 1). The overall crosstalk reduction (R_{ij}) between channels i and j by MESA as compared to CW mode can now be calculated using the crosstalk factors as:

$$R_{ij} = \frac{C_{i\to j}^{\text{CW}} - C_{i\to j}^{\text{MESA}}}{C_{i\to j}^{\text{CW}}} \quad (2)$$

The total crosstalk reduction from Ch1 to Ch2; Ch2 to Ch3 and Ch1 to Ch3 are calculated as 96.4%, 98.32% and 98.57%

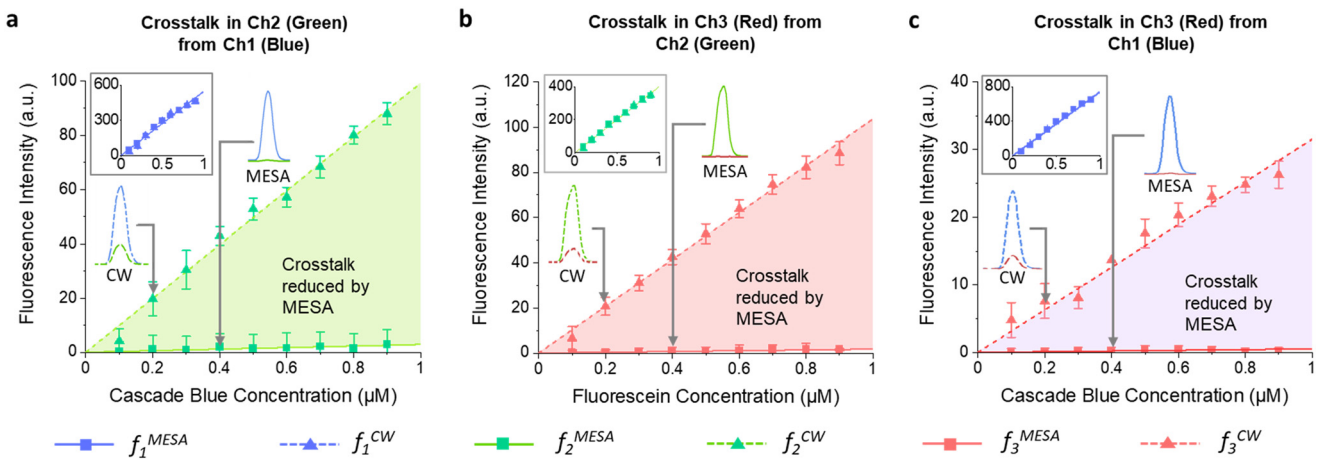

Fig. 3 Crosstalk quantification. a) Droplet mean fluorescence intensity (f) with varying cascade blue concentrations as acquired in blue channel (Ch1) (inset) and green channel (Ch2) in continuous wave (CW) and MESA mode. The shaded area shows the crosstalk in CW mode that is reduced by using the MESA mode. Droplet signal peaks obtained by CW (at 0.2 μM) and MESA (at 0.4 μM) mode are also shown. b) Droplet fluorescence intensity (f) with varying fluorescein concentrations as acquired in green channel (Ch2) (inset) and red channel (Ch3) in CW and MESA mode. c) Droplet fluorescence intensity with varying cascade blue concentrations as acquired in blue channel (Ch1) (inset) and red channel (Ch3) in CW and MESA mode. The error bars in each plot show the standard deviation around mean.

Table 1 Crosstalk factors ($C_{i\to j}$) between the emission channels as calculated from the droplet fluorescence signals using eqn (1) and total crosstalk reduction (R_{ij}) by MESA calculated using eqn (2)

	Description	$C_{i\to j}^{CW}$	$C_{i\to j}^{MESA}$	R_{ij}
$C_{1\to 2}$	Crosstalk in Ch2 (green) from Ch1 (blue)	0.17 ± 0.034	0.006 ± 0.0022	**96.4%**
$C_{2\to 3}$	Crosstalk in Ch3 (red) from Ch2 (green)	0.25 ± 0.029	0.0042 ± 0.0015	**98.32%**
$C_{1\to 3}$	Crosstalk in Ch3 (red) from Ch1 (blue)	0.052 ± 0.02	0.0007 ± 0.0003	**98.57%**

respectively (Table 1). A detailed calculation of crosstalk factors is provided in Tables S1–S3.† The crosstalk factors calculated here are also in agreement with the theoretically estimated crosstalk factors as shown in Table S4.† For theoretical estimations, we developed an interactive tool that simulates crosstalk factors by accounting for all the contributing factors (for *e.g.* emission and excitation spectra of fluorophores, overlap of excitation spectra with excitation laser, overlap of emission spectra with channels, spectral response and gain values of photomultiplier tubes, FRET, optical filter losses *etc.*) (for details see Fig. S3† and "crosstalk calculator" tool available in Software S1†). Note that due to factors like non-uniform spectral response and non-linear gain response of PMTs, non-uniform transmission losses (along the spectra) by all the optical components, difference in quantum yield of fluorophores, difference in laser powers *etc.*, it is difficult to estimate the crosstalk factors with absolute precision. It should also be noted that judiciously selecting the filters in accordance with the fluorophores used (for *e.g.* using narrow band filters or filters whose bandwidth does not include the wavelengths where the spectral overlap is prominent) may help in reducing the crosstalk in CW mode at the cost of reduced signal intensity. However, a significant crosstalk will still persist because it is inherent to the CW fluorescence analysis method mainly due to FRET and excitation overlap (Table S5†). Moreover, the crosstalk will increase further when number of fluorophores and channels is increased in CW mode. MESA, on the other hand, eliminates the very cause of this crosstalk by avoiding all crosstalk components and thus, our method is particularly preferable for multiplexed signal acquisition. The Crosstalk reduction is not 100%, primarily because the acousto-optic modulation is limited in terms of completely blocking the laser

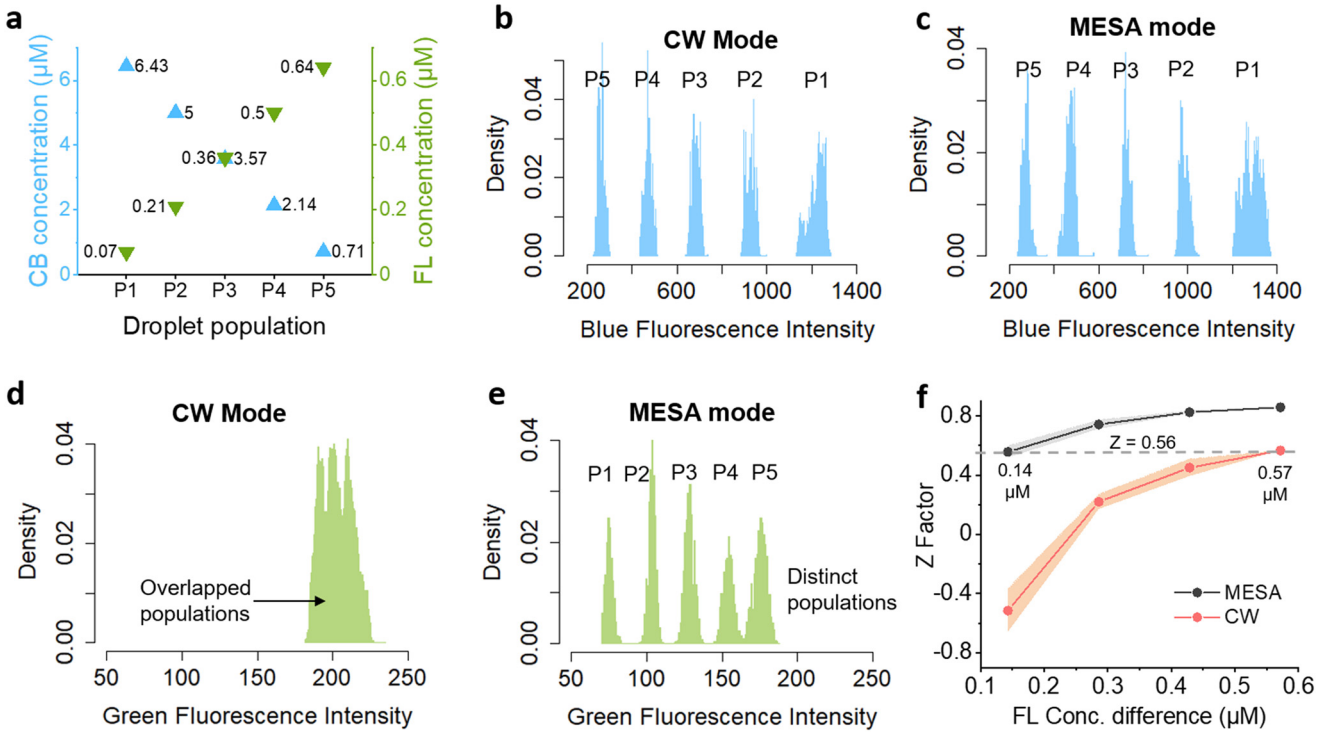

Fig. 4 Improvement in signal resolution by MESA. a) Droplet populations (P1 to P5) where each droplet carries the represented concentrations of CB and FL. Each population consists of more than 200 000 droplets. b) Droplet fluorescence intensity distribution for each population in blue channel (Ch1) as acquired by continuous wave (CW) mode. c) Droplet fluorescence intensity distribution in channel (Ch1) as acquired by MESA mode. d) Droplet fluorescence intensity distribution in green channel (Ch2) as acquired by CW mode, showing overlapped populations. e) Droplet fluorescence intensity distribution in green channel (Ch2) as acquired by MESA mode, showing distinct populations. f) Mean *Z*-factor between the fluorescence intensity distributions of droplet populations separated by various FL concentration differences calculated using eqn (3) (Tables S3 and S4†). The shaded area shows the standard deviation around mean.

radiation.[22] As a result, even at TTL low, there is a small fraction of laser radiation that still excites the fluorophores, which in turn may leak into other channels.

A major benefit of the crosstalk reduction is an improved resolution of multi-color fluorescence populations, which is of particular relevance for barcoding applications.[23–26] To analyze the improvement in resolution by MESA, we used the microfluidic device shown in Fig. 2a to generate five populations of droplets (P1–P5) with discrete concentrations of both cascade blue (CB) and fluorescein (FL) (Fig. 4a). As Ch1 is free of crosstalk in both CW and MESA modes, we used the CB concentration as a control and observed the corresponding FL concentration in the droplets to see the effect of crosstalk in resolving droplet populations. Without the crosstalk, the green fluorescence signals in Ch2 are expected to show discernible populations of droplets with similar concentrations independent of the CB concentration. However, due to crosstalk, the blue fluorescence from CB will leak into green signals, attenuating the effect of FL concentration difference and diminishing the separation between droplet populations. Fig. 4b–e shows the droplet fluorescence signals acquired at 5 equidistant concentrations of the fluorophores in CW and MESA modes. The blue fluorescence by CB showed considerably separated populations in both modes because of the lack of crosstalk in Ch1 (Fig. 4b and c). The similar fluorescence intensity values obtained by both modes for individual CB concentration also demonstrates that the strength of signals acquired by MESA is comparable to that obtained by CW mode (Fig. S4†). In contrast, Ch2 showed overlapped population distributions when using CW mode due to crosstalk from Ch1 (Fig. 4d). In contrast, MESA mode could successfully resolve the green fluorescence into five distinct populations, indicating the improvement in signal resolution by MESA (Fig. 4e). To quantify this improvement in resolution, we compared the *Z*-factors between the FL fluorescence intensity distributions from the populations P1–P5 acquired by CW and MESA modes.[27] The *Z*-factor is a statistical indicator widely used in high-throughput screenings to quantify the separation between two populations where a *Z*-factor greater than 0.5 is considered as excellent separation.[27]

$$Z\text{ factor} = 1 - \frac{3(\sigma_{Pb} + \sigma_{Pa})}{|\mu_{Pb} - \mu_{Pa}|} \quad (3)$$

Here, μ and σ are the mean and standard deviations of the fluorescence intensity distribution of the droplets in population Pa and Pb. For MESA mode, the adjacent populations, *i.e.* concentration difference of 0.14 μM, corresponds to a mean *Z*-factor of 0.56 indicating an excellent separation (Fig. 4f).[27] A detailed calculation of *Z*-factors is presented in Tables S6 and S7.† In contrast, in CW mode, a *Z*-factor greater than 0.5 is achieved only at the highest separation in the experiment *i.e.* a concentration difference of 0.57 μM, which is 4-fold higher than the minimum separation required in MESA mode, demonstrating its higher resolving power (Fig. 4f).

In summary, we present a method for reducing crosstalk between fluorophores and improving signal resolution in the emission channels. We showed that MESA is able to reduce on average 97.75% of crosstalk, when compared to signals obtained with conventional continuous wave method. We further showed that due to reduced crosstalk contribution, MESA has a higher resolving power to differentiate between droplets with closely separated fluorophore concentrations. This is of particular advantage for fluorescence barcoding applications, requiring multiple fluorophores at discrete concentrations to differentiate between numerous fluorescently labelled populations.[23,24,26,28] For example, Brouzes *et al.* encoded a drug library with eight concentrations of a fluorescent dye and used continuous wave mode to differentiate droplet populations that contained different concentrations of mitomycin C for screening its cytotoxic effects on U937 cells.[26] Using MESA instead of CW would allow to increase the number of barcodes to 32 combinations over the same concentration space and up to even 1024 combinations when using a second color.

We conclude that MESA can successfully reduce the spectral overlap induced crosstalk in real-time multi-wavelength florescence analysis. By eliminating the need for any pre-experiment calibration of the instrument, numerical corrections and hydrodynamic focusing of analyte, MESA proves to be a significant development over existing crosstalk mitigating technologies.[7,8]

Data availability

Raw data for all the experiments can be found on **https://doi.org/10.5281/zenodo.6983494**. The "crosstalk calculator" tool is available on Supplementary software 1 or on **https://doi.org/10.5281/zenodo.7706104**.

Conflicts of interest

Parts of the technology described here have been patented. If the patents ever get licensed, the authors might profit financially though the inventor reward programs of the involved institutes.

Acknowledgements

Parts of this work were supported by DFG-Grant ME 3536/9-1.

References

1 K. Matuła, F. Rivello and W. T. S. Huck, Single-Cell Analysis Using Droplet Microfluidics, *Adv. Biosyst.*, 2020, **4**(1), 1900188.
2 S. Sohrabi, N. Kassir and M. K. Moraveji, Droplet microfluidics: fundamentals and its advanced applications, *RSC Adv.*, 2020, **10**(46), 27560–27574.

3 N. Shembekar, C. Chaipan, R. Utharala and C. A. Merten, Droplet-based microfluidics in drug discovery, transcriptomics and high-throughput molecular genetics, *Lab Chip*, 2016, **16**(8), 1314–1331.
4 E. Thews, M. Gerken, R. Eckert, J. Zäpfel, C. Tietz and J. Wrachtrup, Cross Talk Free Fluorescence Cross Correlation Spectroscopy in Live Cells, *Biophys. J.*, 2005, **89**(3), 2069–2076.
5 B. K. Müller, E. Zaychikov, C. Bräuchle and D. C. Lamb, Pulsed Interleaved Excitation, *Biophys. J.*, 2005, **89**(5), 3508–3522.
6 C. Yang, V. Hou, L. Y. Nelson and E. J. Seibel, Mitigating fluorescence spectral overlap in wide-field endoscopic imaging, *J. Biomed. Opt.*, 2013, **18**(8), 086012.
7 S. Chevrier, H. L. Crowell, V. R. T. Zanotelli, S. Engler, M. D. Robinson and B. Bodenmiller, Compensation of Signal Spillover in Suspension and Imaging Mass Cytometry, *Cell Syst.*, 2018, **6**(5), 612–620.e5.
8 C. B. Bagwell and E. G. Adams, Fluorescence Spectral Overlap Compensation for Any Number of Flow Cytometry Parameters, *Ann. N. Y. Acad. Sci.*, 1993, **677**(1), 167–184.
9 N. Shembekar, H. Hu, D. Eustace and C. A. Merten, Single-Cell Droplet Microfluidic Screening for Antibodies Specifically Binding to Target Cells, *Cell Rep.*, 2018, **22**(8), 2206–2215.
10 L. Mazutis, J. Gilbert, W. L. Ung, D. A. Weitz, A. D. Griffiths and J. A. Heyman, Single-cell analysis and sorting using droplet-based microfluidics, *Nat. Protoc.*, 2013, **8**(5), 870–891.
11 A. R. Abate, T. Hung, P. Mary, J. J. Agresti and D. A. Weitz, High-throughput injection with microfluidics using picoinjectors, *Proc. Natl. Acad. Sci. U. S. A.*, 2010, **107**(45), 19163–19166.
12 J. Panwar, A. Autour and C. A. Merten, Design and construction of a microfluidics workstation for high-throughput multi-wavelength fluorescence and transmittance activated droplet analysis and sorting, *Nat. Protoc.*, 2023, **27**, 1–57.
13 H. D. Xi, H. Zheng, W. Guo, A. M. Gañán-Calvo, Y. Ai and C. W. Tsao, *et al.*, Active droplet sorting in microfluidics: a review, *Lab Chip*, 2017, **17**(5), 751–771.
14 J. W. Lichtman and J. A. Conchello, Fluorescence microscopy, *Nat. Methods*, 2005, **2**(12), 910–919.
15 J. Hohlbein, T. D. Craggs and T. Cordes, Alternating-laser excitation: single-molecule FRET and beyond, *Chem. Soc. Rev.*, 2014, **43**(4), 1156–1171.
16 F. Eduati, R. Utharala, D. Madhavan, U. P. Neumann, T. Longerich and T. Cramer, *et al.*, A microfluidics platform for combinatorial drug screening on cancer biopsies, *Nat. Commun.*, 2018, **9**(1), 2434.
17 B. E. Debs, R. Utharala, I. V. Balyasnikova, A. D. Griffiths and C. A. Merten, Functional single-cell hybridoma screening using droplet-based microfluidics, *Proc. Natl. Acad. Sci. U. S. A.*, 2012, **109**(29), 11570–11575.
18 J. L. Madrigal, N. G. Schoepp, L. Xu, C. S. Powell, C. L. Delley and C. A. Siltanen, *et al.*, Characterizing cell interactions at scale with made-to-order droplet ensembles(MODEs), *Proc. Natl. Acad. Sci. U. S. A.*, 2022, **119**(5), e2110867119.
19 W. Becker, Fluorescence lifetime imaging – techniques and applications, *J. Microsc.*, 2012, **247**(2), 119–136.
20 *OptoSpin25 High Speed Filter Wheel*, 89North, available from: **https://www.89north.com/fluorescence-microscopy-products-by-brand/cairn/optospin25-high-speed-filter-wheel/**.
21 *Ultra-Fast Motorised Laser Beam Shutter - Opto-Mechanics - Catalog - Opto-Mechanical Products – Standa*, available from: **https://www.standa.lt/products/catalog/opto_mechanics?item=532**.
22 S. E. Harris, S. T. K. Nieh and R. S. Feigelson, CaMoO4 ELECTRONICALLY TUNABLE OPTICAL FILTER, *Appl. Phys. Lett.*, 1970, **17**(5), 223–225.
23 P. O. Krutzik, M. R. Clutter, A. Trejo and G. P. Nolan, Fluorescent cell barcoding for multiplex flow cytometry, *Curr. Protoc. Cytom.*, 2011, **55**(1), 6–31.
24 E. Z. Macosko, A. Basu, R. Satija, J. Nemesh, K. Shekhar and M. Goldman, *et al.*, Highly Parallel Genome-wide Expression Profiling of Individual Cells Using Nanoliter Droplets, *Cell*, 2015, **161**(5), 1202–1214.
25 Y. Zhao, Z. Xie, H. Gu, L. Jin, X. Zhao and B. Wang, *et al.* Multifunctional photonic crystal barcodes from microfluidics, *NPG Asia Mater.*, 2012, **4**(9), e25.
26 E. Brouzes, M. Medkova, N. Savenelli, D. Marran, M. Twardowski and J. B. Hutchison, *et al.*, Droplet microfluidic technology for single-cell high-throughput screening, *Proc. Natl. Acad. Sci. U. S. A.*, 2009, **106**(34), 14195–14200.
27 J. H. Zhang, T. D. Y. Chung and K. R. Oldenburg, A Simple Statistical Parameter for Use in Evaluation and Validation of High Throughput Screening Assays, *SLAS Discovery*, 1999, **4**(2), 67–73.
28 S. Song, M. Manook, J. Kwun, A. M. Jackson, S. J. Knechtle and G. Kelsoe, A cell-based multiplex immunoassay platform using fluorescent protein-barcoded reporter cell lines, *Commun. Biol.*, 2021, **4**(1), 1–9.